Electronic Supplementary Information for

Ultrafine AuCu nanowires for electrocatalytic nitrogen fixation

Hongjing Wang, Lin Cui, Songliang Liu, Hongjie Yu, Kai Deng, You Xu, Xiaonian Li,

Ziqiang Wang* and Liang Wang*

State Key Laboratory Breeding Base of Green-Chemical Synthesis Technology, College of Chemical Engineering, Zhejiang University of Technology, Hangzhou 310014, P. R. China.

Corresponding authors

*E-mails: zqwang@zjut.edu.cn; wangliang@zjut.edu.cn

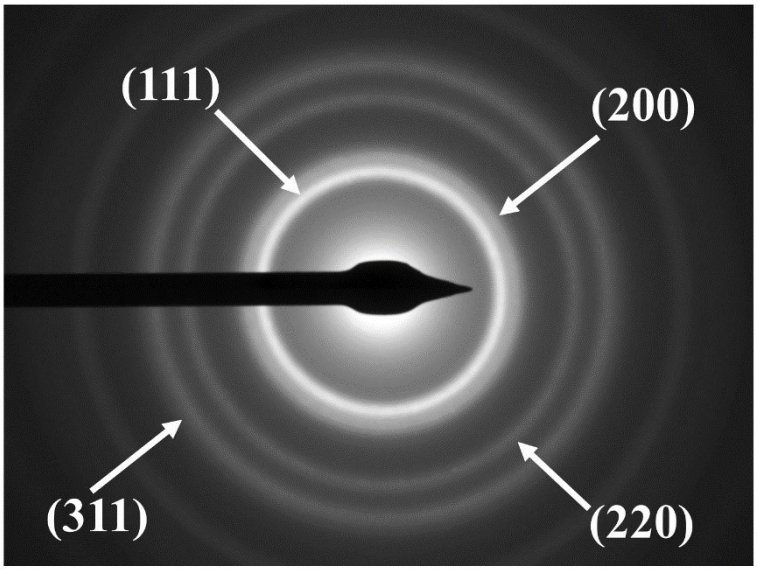

Fig. S1 SAED pattern of the AuCu NWs.

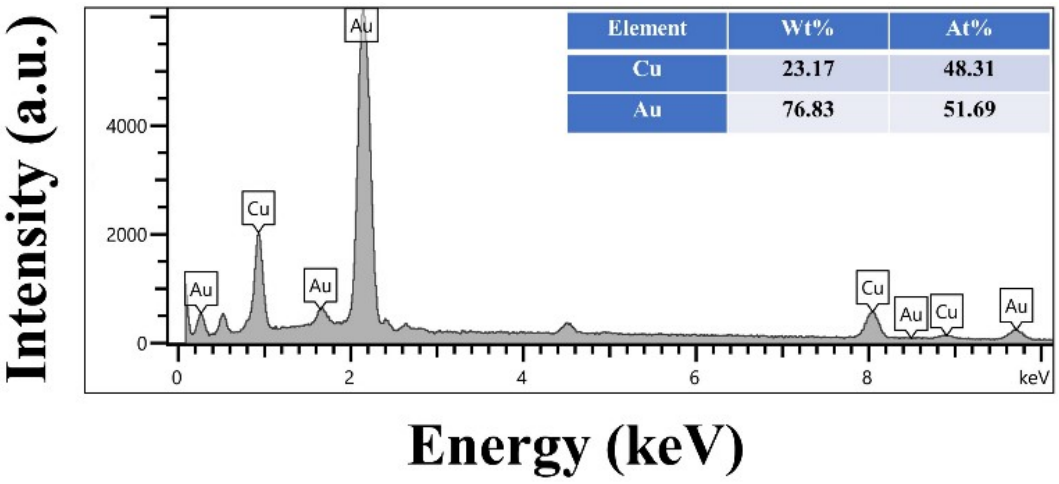

Fig. S2 The EDX spectrum of the AuCu NWs and corresponding mass and atomic ratios.

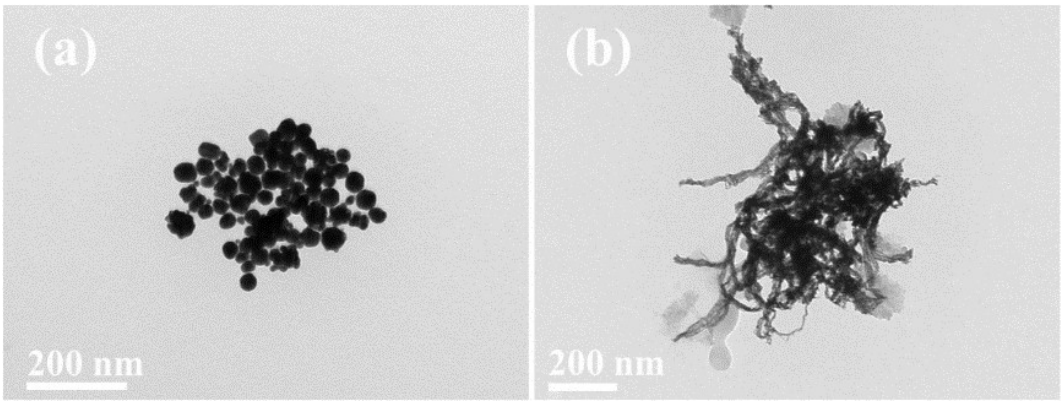

Fig. S3 TEM images of the samples prepared with (a) 0 mg of 4-aminopyridine and (b) 94 mg of 4-aminopyridine under the typical synthesis conditions.

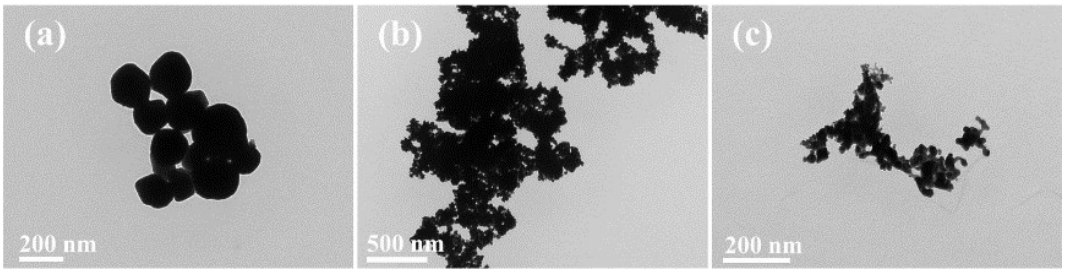

Fig. S4 TEM images of the samples prepared with (a) DM-970, (b) F127, and (c) PS-b-PMMA under the typical synthesis conditions.

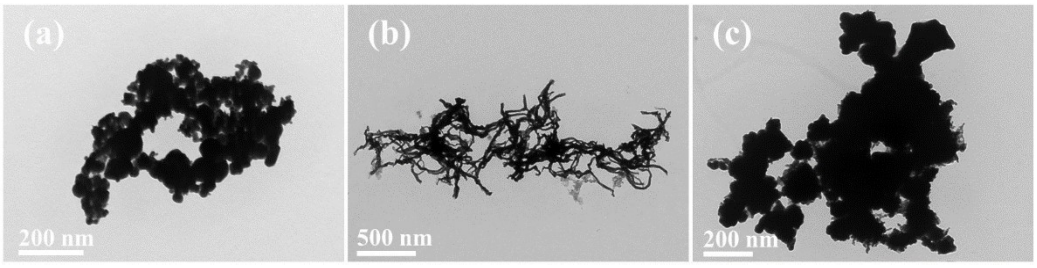

Fig. S5 TEM images of samples prepared (a) without AA, from (b) HCOOH and (c) glucose under the typical synthesis conditions.

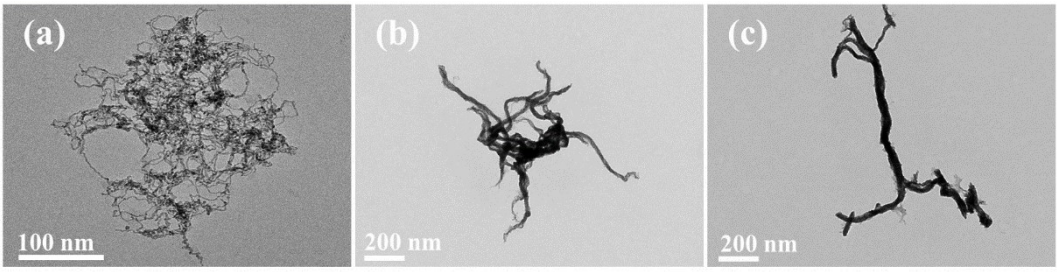

Fig. S6 TEM images of different samples prepared with different amounts of metal precursors under the same conditions. The amount of added metal precursors for $HAuCl_4$ and $CuCl_2$ is (a) 2 and 0 mL (Au NWs); (b) 1.5 and 0.5 mL ($Au_{1.5}Cu_{0.5}$ NWs); (c) 0.5 and 1.5 mL ($Au_{0.5}Cu_{1.5}$ NWs).

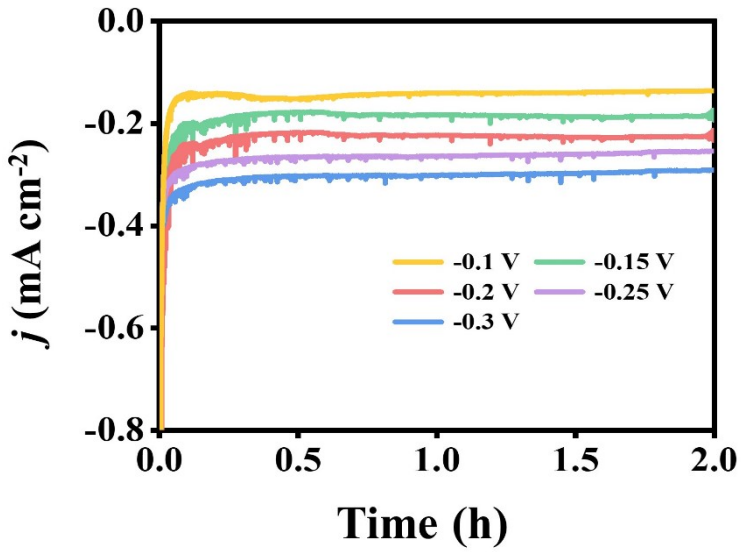

Fig. S7 Chronoamperometry curves of AuCu NWs for 2 h at selected potentials.

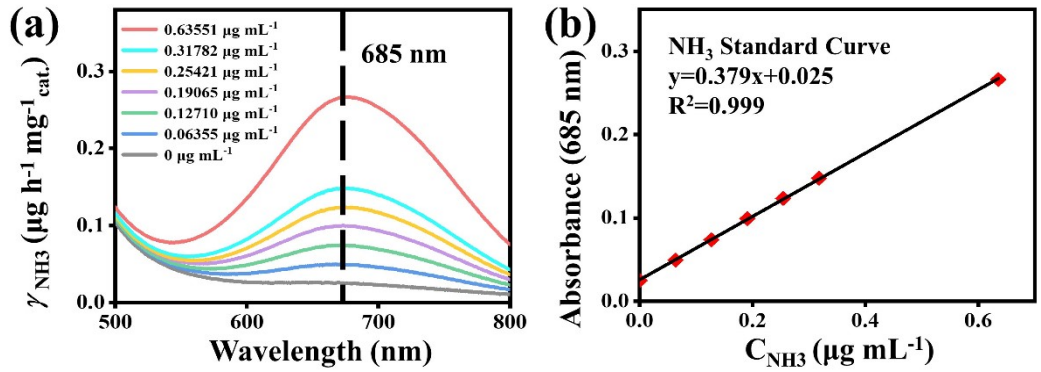

Fig. S8 (a) UV-vis spectra at various ammonia concentrations after being incubated for 1 h at room temperature, and (b) the corresponding calibration curve.

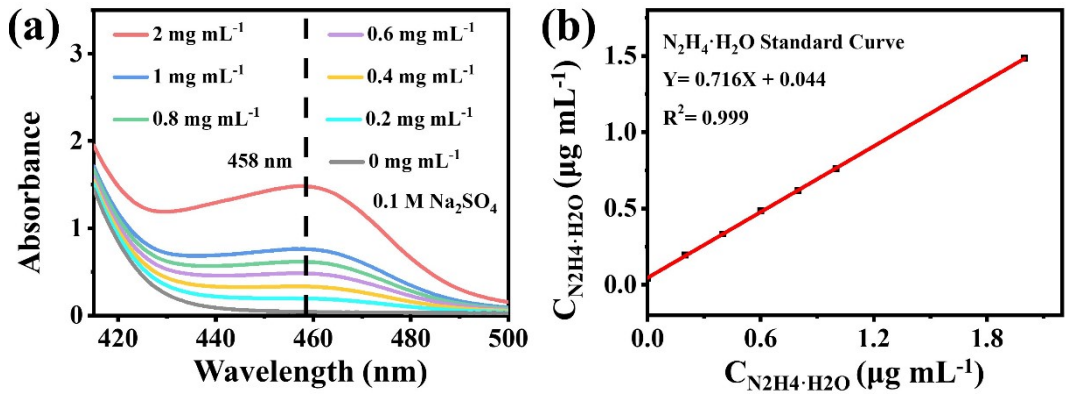

Fig. S9 (a) UV-vis spectra at various hydrazine concentrations after being incubated for 15 min under ambient conditions, and (b) the corresponding calibration curve.

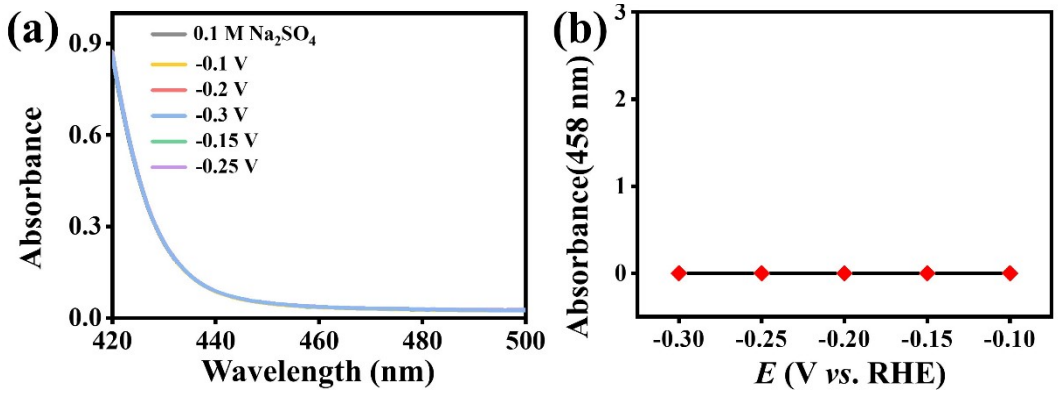

Fig. S10 (a) UV-vis spectra of the electrolytes after 2 h electrolysis at different potentials, and (b) the N_2H_4 concentration of the electrolyte.

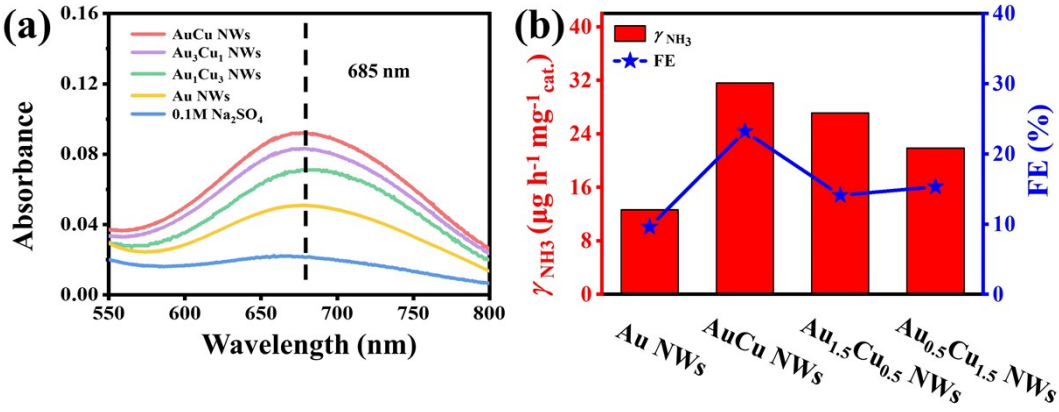

Fig. S11. UV-vis absorbance spectra of different samples at −0.2 V, and (b) corresponding r_{NH3} and FE.

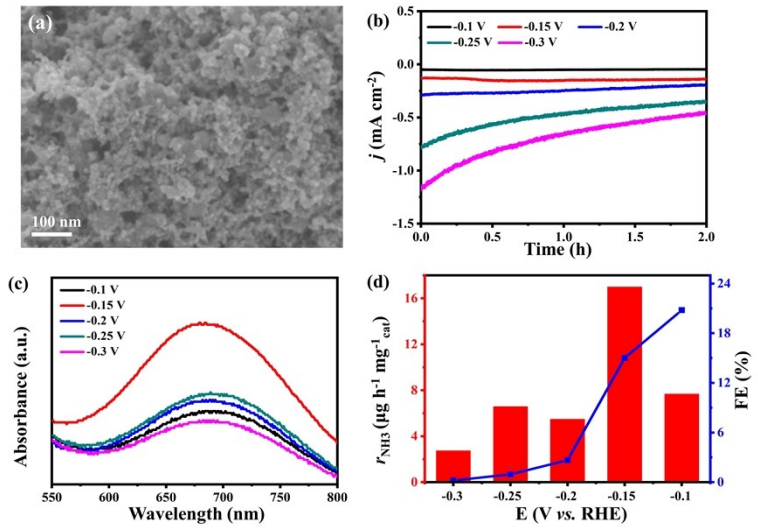

Fig. S12 SEM image of AuCu NPs (a). The i-t curve of AuCu NPs at different potentials (b), and corresponding UV-vis absorbance spectra of electrolysis solutions (c) and r_{NH3} and FE (d).

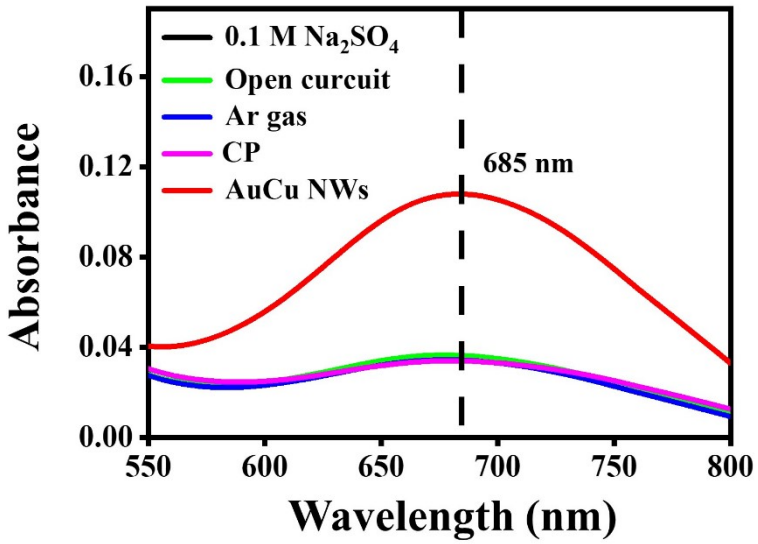

Fig. S13 UV-vis absorption spectra of electrolytes under different conditions.

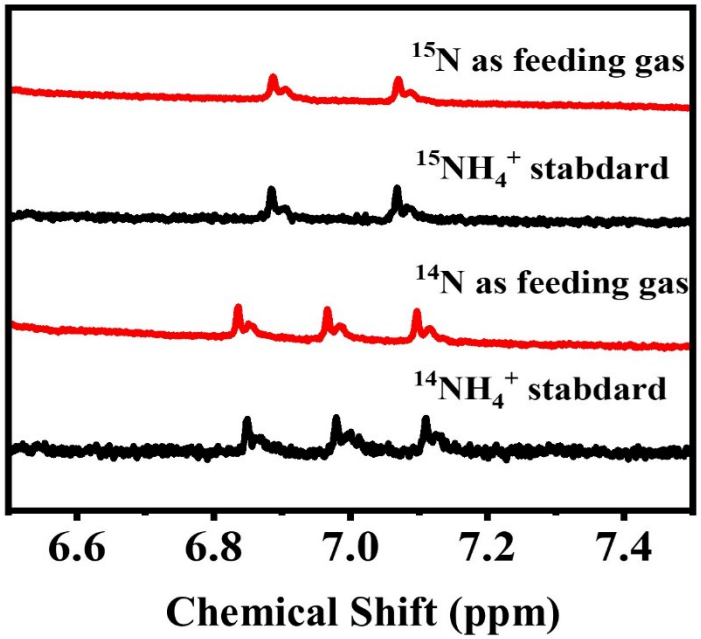

Fig. S14 ^{1}H-NMR spectra of standard $^{14}NH_4^+$ and $^{15}NH_4^+$ solutions, and the electrolytes produced from the NRR using $^{14}N_2$ and $^{15}N_2$ as the N_2 source.

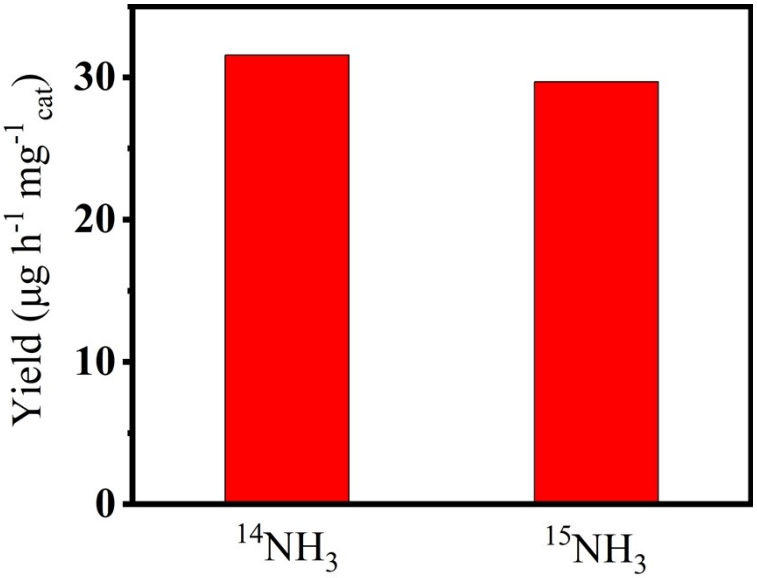

Fig. S15 The yield of formed $^{14}NH_3$ and $^{15}NH_4$ using $^{14}N_2$ and $^{15}N_2$ as the N_2 source.

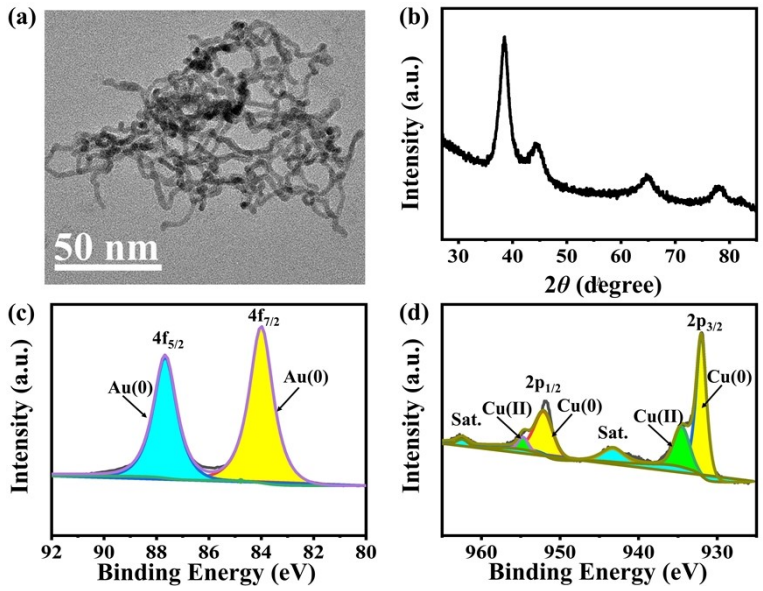

Fig. S16 TEM image (a), XRD pattern (b) and XPS spectra (c, d) of AuCu NWs after catalytic stability test.

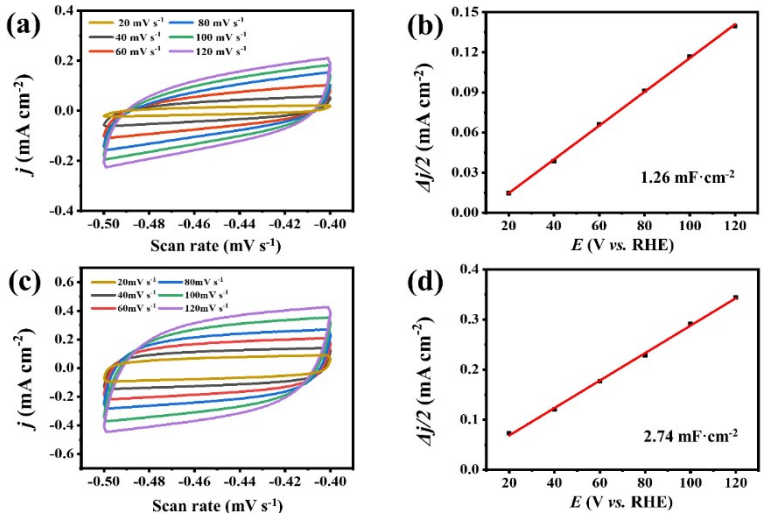

Fig. S17 CV curves of Au NWs (a) and AuCu NWs (b) in the range of −0.40 and −0.50 V. Capacitive current densities derived from CVs at −0.45 V against scan rates for Au NWs (c) and AuCu NWs (d).

Table S1 The NRR performance comparisons of the AuCu NWs with the recently reported catalysts under ambient conditions.

Catalyst	Electrolyte	NH_3 yield	FE (%)	Ref.
AuCu NWs	**0.1 M Na_2SO_4**	**31.57 μg h^{-1} $mg^{-1}_{cat.}$**	**22.1**	**This work**
AuCu/ZIF-8	0.1 M Na_2SO_4	14.50 μg h^{-1} $mg^{-1}_{cat.}$	6.70	1
S/Au NWs	0.1 M Na_2SO_4	21.04 μg h^{-1} $mg^{-1}_{cat.}$	15.34	2
AuPdP NWs	0.1 M Na_2SO_4	18.78 μg h^{-1} $mg^{-1}_{cat.}$	15.44	3
Ag_3Cu BPNs	0.1 M Na_2SO_4	24.59 μg h^{-1} $mg^{-1}_{cat.}$	13.28	4
Pd NPs	0.1 M Na_2SO_4	24.12 μg h^{-1} $mg^{-1}_{cat.}$	9.49	5
nPd/NF	0.1 M Na_2SO_4	18.27 μg h^{-1} $mg^{-1}_{cat.}$	10.36	6
AuPd NSs	0.1 M Na_2SO_4	16.9 μg $h^{-1}mg^{-1}_{cat.}$	15.9	7
AuCuB PNSs	0.1 M Na_2SO_4	13.2 μg h^{-1} $mg^{-1}_{cat.}$	12.78	8

References

1. X.-W. Lv , L. Wang, G. Wang, R. Hao, J.-T. Ren, X. Liu, P. N. Duchesne, Y. Liu, W. Li, Z.-Y. Yuan and G. A. Ozin, ZIF-supported AuCu nanoalloy for ammonia electrosynthesis from nitrogen and thin air, *J. Mater. Chem. A*, 2020, **8**, 8868-8874.
2. H. Wang, D. Yang, S. Liu, S. Yin, H. Yu, Y. Xu, X. Li, Z. Wang and L. Wang, Amorphous sulfur decorated gold nanowires as efficient electrocatalysts toward ambient ammonia synthesis, *ACS Sustainable Chem. Eng.*, 2019, **7**, 19969-19974.
3. H. Wang, D. Yang, S. Liu, S. Yin, Y. Xu, X. Li, Z. Wang and L. Wang, Metal–nonmetal one-dimensional electrocatalyst: AuPdP nanowires for ambient nitrogen reduction to ammonia, *ACS Sustainable Chem. Eng.*, 2019, **7**, 15772-15777.
4. H. Yu, Z. Wang, D. Yang, X. Qian, Y. Xu, H. Wang and L. Wang, Bimetallic Ag_3Cu porous networks for ambient electrolysis of nitrogen to ammonia, *J. Mater. Chem. A*, 2019, **7**, 12526-12531.
5. G. Deng, T. Wang, A. A. Alshehri, K. A. Alzahrani, Y. Wang, H. Ye, Y. Luo and X. Sun, Improving the electrocatalytic N_2 reduction activity of Pd nanoparticles through surface modification, *J. Mater. Chem. A*, 2019, **7**, 21674-21677.
6. Z. Wang, Z. Dai, H. Yu, H. Zhang, W. Tian, Y. Xu, X. Li, L. Wang and H. Wang, Pore-size-tuned Pd films grown on Ni foam as an advanced catalyst for electrosynthesis of ammonia, *ACS Sustainable Chem. Eng.*, 2020, **8**, 11827-11833.
7. S. Yin, S. Liu, H. Zhang, S. Jiao, Y. Xu, Z. Wang, X. Li, L. Wang and H. Wang, Engineering one-dimensional AuPd nanospikes for efficient electrocatalytic nitrogen fixation, *ACS Appl. Mater. Interfaces*, 2021, **13**, 20233-20239.

8. Z. Wang, J. Niu, Y. Xu, L. Wang, H. Wang and H. Liu, Effects of AuCuB catalysts with porous nanostructures on electrosynthesis of ammonia, *ACS Sustainable Chem. Eng.*, 2020, **8**, 12588-12594.